All-Polymer Photonic Microcavities Doped with Perylene Bisimide J-Aggregates

Paola Lova, Vincenzo Grande, Giovanni Manfredi, Maddalena Patrini, Stefanie Herbst, Frank Würthner, and Davide Comoretto**

Thanks to exciting chemical and optical features, perylene bisimide J-aggregates are ideal candidates to be employed for high-performance plastic photonic devices. However, they generally tend to form π–π stacked H-aggregates that are unsuitable for implementation in polymer resonant cavities. In this work, the efficient compatibilization of a tailored perylene bisimide forming robust J-aggregated supramolecular polymers into amorphous polypropylene is introduced. The new nanocomposite is then implemented into an all-polymer planar microcavity, which provides strong and directional spectral redistribution of the J-aggregate photoluminescence, due to a strong modification of the photonic states. A systematic analysis of the photoemitting processes, including photoluminescence decay and quantum yields, shows that the optical confinement in the polymeric microcavity does not introduce any additional nonradiative de-excitation pathways to those already found in the J-aggregate nanocomposite film and pave the way to PBI-based high-performance plastic photonic devices.

1. Introduction

Since the discovery of pseudoisocyanine J-aggregates in the 1930s,[1] several synthetic and natural dye aggregates have been developed and investigated.[2] Thanks to outstanding photoemitting properties[3] that include super-radiance,[4] high absorbance, and sharp emission,[5] J-aggregates entered in the spotlight for applications in anti-fraud systems,[6] and biological imaging[7] and for optoelectronic devices such as light emitting diodes,[8] lasers,[9] optical switches,[9] colorimetric sensors,[10] and for the achievement of strong-coupling effects.[11] Among these dyes, perylene bisimides (PBIs, in red in **Figure 1**) display exceptional photochemical stability against photo-oxidation that is bestowed by two electron withdrawing dicarboximide units.[5,12] Moreover, a substantial rigidity of the PBI core imparts high absorption coefficients around 70 000 M^{-1} cm^{-1} in the wavelength region 510–540 nm, inefficient triplet formation, and photoluminescence quantum yields (PL QYs) close to unity in molecular solutions[13] that result overall in amplified stimulated emission from 0–1 and 0–2 vibronic transitions.[14] In addition, relatively easy chemical functionalization at the perylene core allows to variably tune chemical and optoelectronic features.[13a] Accordingly, core-substitution is known to introduce considerable twist of the aromatic core[15] leading, on one hand, to a small reduction of QY for the monomeric PBI solution;[13a,16] on the other hand, to an enhancement of the QY in the solid state by preventing H-aggregates formation.[17]

The large interest in the supramolecular arrangement of PBIs owes to its enormous impact on their optical features and photophysics. According to Kasha's theory, Frenkel excitons may couple in either H- or J-type aggregates.[18] H-type coupling leads to a blueshifted optical transition with lower QY with respect to the monomer, which makes H-aggregates highly undesired for fluorescence-based applications. Conversely, increased oscillator strength of the highest Frenkel exciton state is predicted for J-aggregates, resulting in red-shifted and narrower absorption and photoluminescence bands compared to the monomer ones.[5] Additionally, hyperchromicity and super-radiance that are also predicted for J-type coupling[5] make them highly desired for photonic applications.

In general, the large tendency of PBIs toward aggregation is principally caused by the extended flat aromatic core.[13a] During the last 20 years, such feature has been widely explored to build up supramolecular functional architectures in solution and in condensed phase.[13a] However, strong π–π interactions typically force the arrangement into the lower emissive H- aggregate[19] and introduces additional radiationless pathways, ultimately

P. Lova, G. Manfredi, Prof. D. Comoretto
Dipartimento di Chimica e Chimica industriale
Università degli Studi di Genova
via Dodecaneso 31, 16146 Genova, Italy
E-mail: davide.comoretto@unige.it

V. Grande, S. Herbst, Prof. F. Würthner
Institut für Organische Chemie
Universität Würzburg
Am Hubland, 97074 Würzburg, Germany
E-mail: wuerthner@uni-wuerzburg.de

V. Grande, S. Herbst, Prof. F. Würthner
Center for Nanosystems Chemistry
and Bavarian Polymer Institute (BPI)
Theodor-Boveri-Weg, 97074 Würzburg, Germany

M. Patrini
Dipartimento di Fisica
Università degli Studi di Pavia
via A. Bassi, 6, 27100 Pavia, Italy

The ORCID identification number(s) for the author(s) of this article can be found under https://doi.org/10.1002/adom.201700523.

DOI: 10.1002/adom.201700523

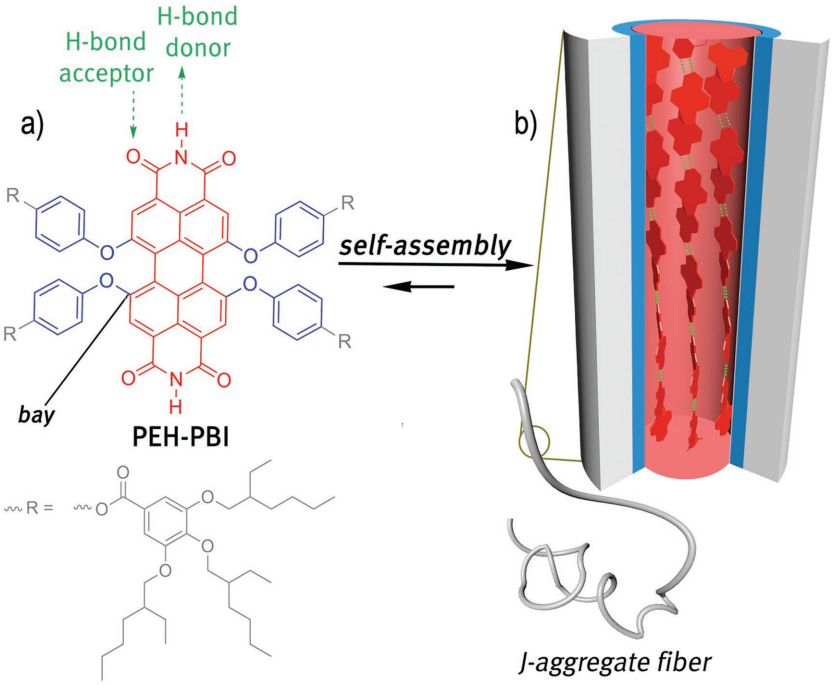

Figure 1. a) Chemical structure of PEH-PBI as a monomer (in organic solvents such as toluene) and b) the hydrogen bond directed J-type aggregate (formed in *n*-hexane). 2-Ethylhexyl substituents have been used as racemic mixture. Hydrogen bonds, displayed in green, direct the formation of the triple-stranded J-aggregate.

resulting in a dramatic suppression of the PL.[20] Indeed, PBI J-aggregates are not easily accessible but could only be achieved by a combination of tetra-substitution with bulky substituents in the bay positions and free imide moieties that trigger the formation of a hydrogen-bonded supramolecular polymer, as shown in Figure 1.[21]

Thanks to the unique aggregate robustness combined with the outstanding optical features, these new PBIs attracted considerable interest for the integration of easily processable supramolecular J-aggregates into polymer matrices. Indeed, the capability to induce J-aggregation into polymer solutions aiming at processable materials is promising for the integration of solid-state active media into plastic photonic devices such as in lasing microcavity. On the other hand, to the best of our knowledge, PBI J-aggregates have never been implemented into all-polymer matrices and structures,[22] while only few bare PBI J-aggregate solid state films have been reported so far.[13a,23] In this regard, Díaz-García's group reported distributed feedback structures made of molecular PBIs embedded in a polystyrene matrix as gain medium,[24] and Martínez-Pastor's group demonstrated highly efficient amplified stimulated emission by molecular PBI in poly(methyl methacrylate).[25] Moreover, lasing effect from PBI J-aggregates still remains a challenging goal. To the best of our knowledge, it has only been demonstrated for single-crystal J-aggregates of *N,N′*-bis(1-ethylpropyl)-2,5,8,11-tetrakis(*p*-methyl-phenyl)-perylenebisimide hexagonal microdisks acting as whispering galleries and appears unsuitable for implementation in technology relevant plastic devices.[23b] The inclusion of PBI J-aggregates into polymer matrices still remains an open issue and an engaging challenge.[26] Polymer matrices raise in fact interesting issues regarding mutual dispersion interactions between the aggregates and the polymer itself that, ultimately, may affect compatibility, processability, and photophysical properties.

Polymer photonic crystals (PhCs) are viable media to achieve plastic devices based on PBI J-aggregates. These materials have been already demonstrated very efficient for photoluminescence enhancement[27] and directional control,[28] lasing action,[29] switching,[30] and sensing.[31] Among them, monodimensional multilayered structures represent the simplest system from the fabrication point of view. Moreover, compared to the hardly scalable fabrication of systems with higher dimensionality, large-area multilayered all-polymer PhCs for efficient photoemission control in distributed feedback structures and microcavity are already industrially fabricated via coextrusion.[32]

In this work, we demonstrate a proof-of-concept all-polymer microcavity embedding PBI J-aggregates loaded into a polymer matrix to investigate photoluminescence intensity enhancement and its directional control. PL lifetime and QY will also be discussed to evaluate light extraction effects. For these studies, a new PBI bearing 2-ethylhexyl-substituted gallic acid residues at *para*-positions of the phenoxy-functionalized PBI (named PEH-PBI, Figure 1) has been developed. By means of 12 bulky branched ethylhexyl groups this dye as well as its aggregates become highly soluble and can be incorporated even at high concentrations into polymeric matrices. The typical slip-stack arrangement of the PBI cores into the supramolecular J-aggregate has shown to be responsible for intriguing optical and photophysical properties,[33] such as the exciton migration along a single supramolecular fiber.

2. Results and Discussion

2.1. Microcavity Fabrication and Optical Properties

Like other PBI J-aggregates[21] also PEH-PBI J-aggregates only form in low-polarity environments, where hydrogen bonds are sufficiently strong. Thus, under dilute conditions ($<0.1 \times 10^{-3}$ M) as given in optical spectroscopy experiments already in toluene, a solvent of intermediate polarity, PEH-PBI dissolves in the monomer state with the typical absorption band peaked at $\lambda_{max} = 563$ nm. Upon increasing the content of non-polar *n*-hexane, the monomer band decreases while a nearly 70 nm redshifted band ($\lambda_{max} = 630$ nm) appears in the spectrum (Figure S1, Supporting Information). This band is ascribed to the presence of a J-aggregate and can be understood as a result of the exciton coupling between the PBI dyes' transition dipole moments in accordance with our previous work on related J-aggregates.[21] The formation of the supramolecular polymer

in *n*-hexane could also be confirmed by atomic force microscopy (AFM) which revealed the formation of nanofibers with length up to several micrometers (Figure S2, Supporting Information), similar to what was observed with other structurally related tetraphenoxy-substituted PBIs.[22,23] The formation of the hydrogen-bonded structure has been additionally proven by Fourier transform infra red (FTIR) spectroscopy which exhibited a remarkable shift of the N—H and imide C=O stretchings to lower energy, thereby supporting the formation of a hydrogen-bonded structure in good analogy with previously reported PBI J-aggregate structure (Figure S3, Supporting Information).[23a]

To embed the J-aggregate fibers into a polymer matrix, the monomeric PEH-PBI was dispersed into a solution of amorphous polypropylene (aPP) and *n*-hexane as described in the Experimental Section. To favor PEH-PBI aggregation during the deposition of the microcavity layer, *n*-hexane was added dropwise to the solution until its color changed from red to blue, indicating the formation of the supramolecular aggregate. The aPP matrix prevents the washout of the dye during the deposition of the subsequent microcavity layers and allows smooth surfaces typical of spun-cast polymers and nanocomposite films.[31b,34] aPP was chosen among commodity polymers because of its good filmability, compatibility with the deposition of the other components of the microcavity, and capability to be blended with PEH-PBI J-aggregates. Indeed, polar polymers such as polyvinyl alcohol, poly(acrylic acid) (PAA), and cellulose acetate cannot be dissolved by the PEH-PBI nonpolar organic solvents. Conversely, aromatic polymers such as polystyrene and poly(vinyl carbazole) do not allow good dispersion of PEH-PBI J-aggregates and favor phase segregation and washout of the J-aggregates during the deposition of the top microcavity layers. Furthermore, the nonpolar aliphatic nature of aPP allows good solubility and convenient stabilization of the J-aggregate dispersion.

Figure 2 shows the absorbance (continuous line) and fluorescence (dashed line) spectra of PEH-PBI:aPP nanocomposite (blue lines in Figure 2) and compares them with the corresponding data for PEH-PBI J-aggregates in solution (red lines in Figure 2). In the latter sample, the J-aggregates show an absorption peak at 630 nm with 14 meV full width at half maximum (FWHM). This intense peak is followed by a shoulder at 555 nm, which is assigned to residual monomeric PEH-PBI, and a band at 450 nm, attributed to higher energy transitions (see Figure S1, Supporting Information). The solution of the J-aggregate shows a sharp fluorescence peak at 657 nm with FWHM of 11 meV. When the J-aggregate is embedded into aPP and casted on a substrate, its absorption spectrum is bathochromically shifted with respect to the solution, showing the maximum of the main absorption peak at 636 nm (blue continuous line in Figure 2). The background of the spectrum is modulated by interference fringes, which testify the very good quality of the nanocomposite film. Similarly, the fluorescence spectrum of the composite thin film is also bathochromically shifted with respect to the solution and peaked at 661 nm. The FWHM of both absorption and fluorescence spectra is very similar to that observed for the PEH-PBI J-aggregates in solution proving that no relevant changes, such as the reorientation of the dyes into H-aggregates, occur in the solid state.

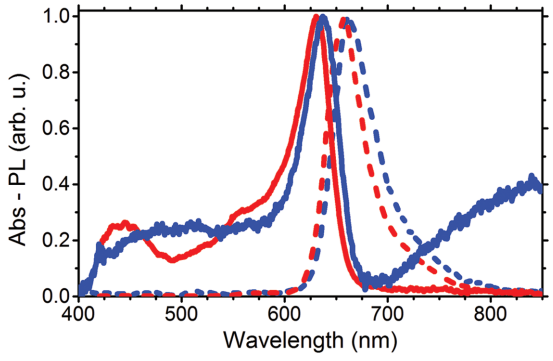

Figure 2. Normalized absorbance (full line) and PL (dashed line) spectra of PEH-PBI J-aggregate in toluene/*n*-hexane solution (red) and aPP composite (blue).

The good processability of PEH-PBI J-aggregates:aPP composite ensures optically good thin films that are suitable for the fabrication of planar microcavities. To manufacture the microcavity structure, the nanocomposite film was spun-cast on top of a distributed Bragg reflector (DBR) made of 40 alternated thin films of poly(*N*-vinylcarbazole) (PVK) and PAA acting as the high ($n \approx 1.68$) and the low ($n \approx 1.51$) refractive index media, respectively. Then, additional 20 periods of PAA:PVK were spun-cast on top of the structure as sketched in **Figure 3**a.

A detailed knowledge of the spectral dispersion of the complex refractive indexes of the materials composing the microcavity is needed for its engineering. While the refractive index of PVK is known,[35] PAA, aPP, and the PEH-PBI:aPP blend indexes have not been investigated yet. Figure S4 (Supporting Information) describes the refractive index dispersion for these materials as determined by spectroscopic ellipsometry characterization. In the visible and near-infrared spectral regions, the refractive index of PAA shows a low dispersion with $n \approx 1.52$ at 600 nm and negligible extinction coefficient. aPP shows a similar behavior but slightly lower refractive index that approaches 1.47 at 600 nm. Loading the J-aggregates in the aPP, their absorption (see also Figure 2) is clearly detected at 630 nm in the complex refractive index dispersion (Figure S4b, Supporting Information, red line). Moreover, a slight increase of the blend refractive index up to $\Delta n = 0.03$ with respect to aPP is observed in the entire spectral range.

Figure 3b shows the reflectance spectra of a PEH-PBI microcavity as collected from different spots of the sample surface. The broad peak positioned between 700 and 770 nm is linked to the DBRs photonic bandgap (PBG).[36] Its FWHM is mainly related to the dielectric contrast between PVK and PAA. The background of the spectra is dominated by a progression of interference fringes, which demonstrates the optimum control of thickness over the sample. The spectra show a minimum in the reflectance peak at ≈725 nm assigned to the cavity mode. This optical mode is allowed to photon propagation thanks to the cavity layer that constitutes a periodicity defect in the photonic structure. The homogeneity of the microcavity, which is constituted by 81 spun-cast layers over 30 mm of diameter, is testified by the superimposition of the spectra collected for the eight spots of the sample surface (Figure 3b).

The good optical quality of the microcavities is also confirmed by angle-resolved transmittance spectra for both P- and

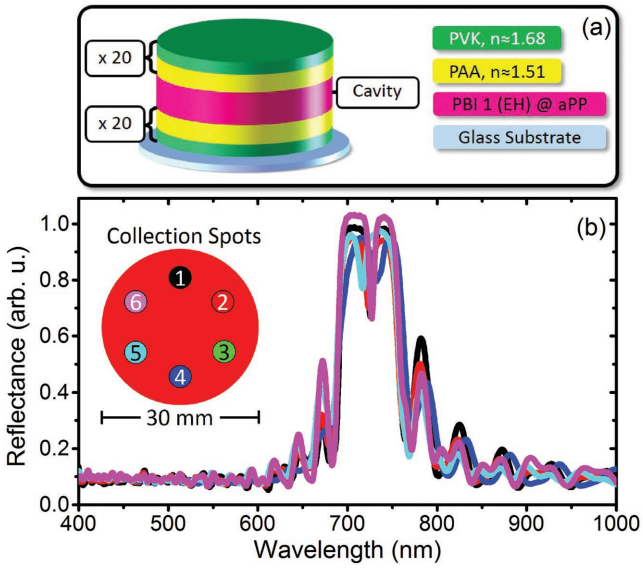

Figure 3. a) Scheme of the microcavity. b) Reflectance spectra collected in different spots of the sample.

S-polarization reported in Figure S5 (Supporting Information). Here, the experimental spectra are in full agreement with those calculated via transfer matrix method.[37] For P-polarization the stop-band width is reduced at the Brewster's angle, while no significant effects on the PBG width are observed for S-polarization. The spectra were simulated using the refractive index dispersion previously discussed. The simulation allowed assessing layer thickness values of 92 nm for PVK, 139 nm for PAA, and 241 nm for PEH-PBI:aPP nanocomposites.

2.2. Microcavity Fluorescence: Enhancement Effects and Directionality

Figure 4a,b compares the microcavity transmittance and fluorescence spectra. The cavity mode previously observed at ≈725 nm (Figure 3b) strongly affects the PEH-PBI J-aggregates fluorescence. The photoluminescence spectrum of the bare J-aggregates:aPP composite is relatively broad and ranges from ≈625 to 800 nm with maximum intensity at 659 nm. In the microcavity, the emission intensity of the J-aggregates:aPP composite is deeply reduced at the PBG wavelengths (690–760 nm, Figure 4a,b), while it is strongly enhanced at the cavity mode wavelength at ≈725 nm. The interference fringes observed in the transmittance spectrum weakly modulate the photoluminescence. Because of the angular dispersion of the PBG and of the cavity mode (Figure S5, Supporting Information), the enhanced peak shifts toward lower wavelength increasing the collection angle (Figure 4c). These data unambiguously demonstrate that the variations in the J-aggregate emission profile are correlated to the photonic structure. Indeed, for collection angle above 45°, the PBG does not spectrally overlap the PEH-PBI PL anymore, and its emission spectrum remains substantially

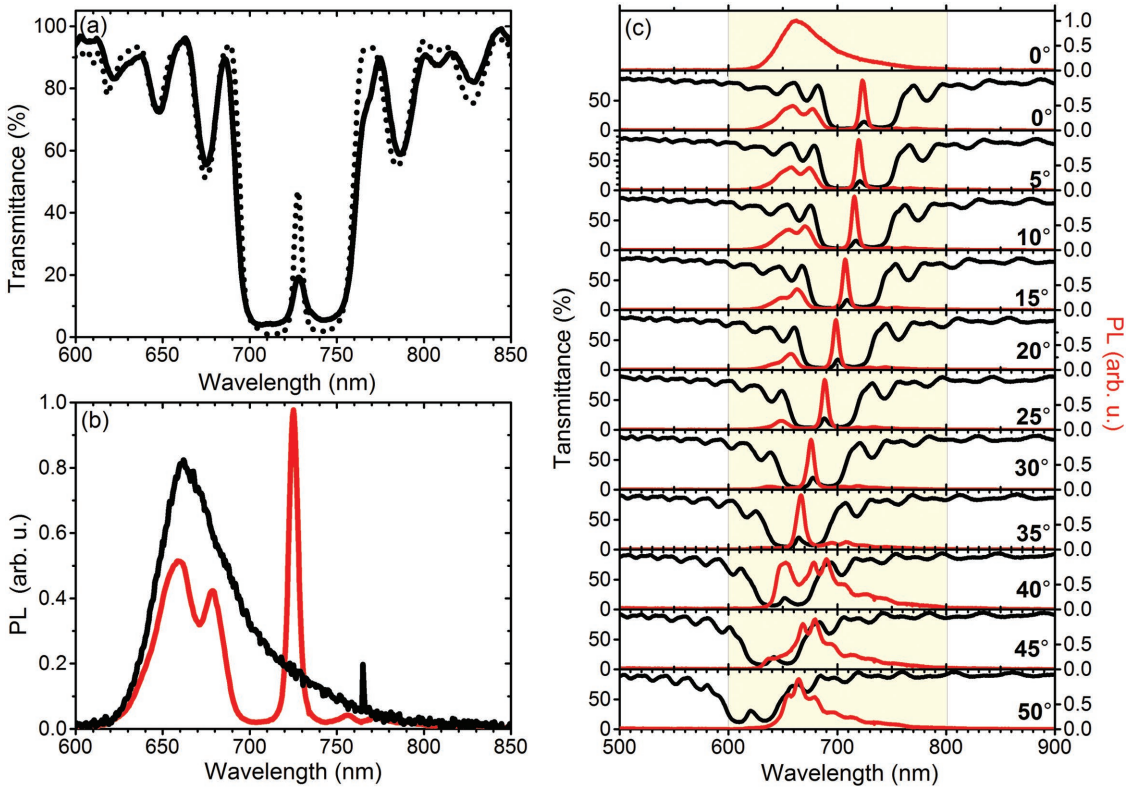

Figure 4. a) Calculated (dashed lines) and experimental (continuous lines) transmittance spectra of the microcavity. b) PL spectra of Reference 1 (black line) and microcavity (red line). c) Angular dispersion of the microcavity transmittance and normalized fluorescence spectra.

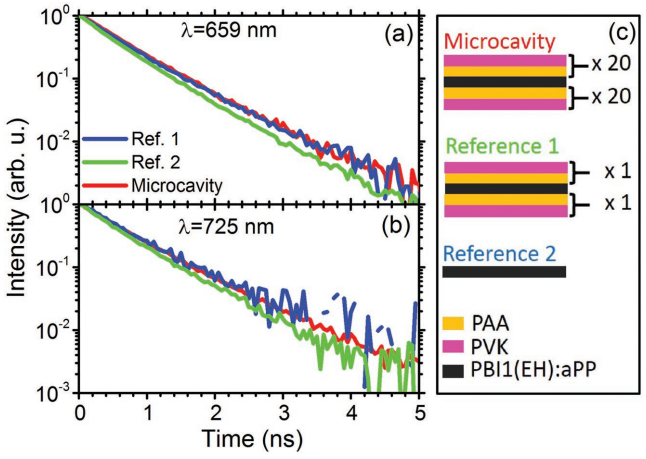

Figure 5. PEH-PBI:aPP composite PL decay kinetics in the nanosecond time regime at a) 659 nm (PEH-PBI J-aggregates PL maximum) and b) at 725 nm (cavity mode). Red line, microcavity; green line, Reference 1; blue line, Reference 2. c) Comparison of the structure for the microcavity and for the reference samples 1 and 2.

unchanged. The microcavity finesse (quality factor, $Q = \lambda/\Delta\lambda$) can be evaluated analyzing the spectral FWHM of the enhanced PL peak that amounts to 6.7 nm, and the quality factor $Q = 107$. This value is in good agreement with data reported for asymmetric microcavities made by metallic and inorganic dielectric mirrors.[38]

In addition to the spectral redistribution of the PL oscillator strength, already discussed for many fluorescing systems,[29] this work analyzes PL enhancement effects. At the cavity mode wavelength, the PL intensity is increased by a factor of 5 with respect to a reference sample fabricated using the same conditions (Reference 1, see the Experimental Section and **Figure 5**c). Figure S6 (Supporting Information) shows the ratio spectrum between the PL of the microcavity and the reference (PL_{cav}/PL_{ref}) as a function of the collection angle. The spectral ratio shows an enhancement at the cavity mode $\left(\frac{PL_{cav}}{PL_{ref}} > 1\right)$ and a suppression at the PBG spectral regions $\left(\frac{PL_{cav}}{PL_{ref}} < 1\right)$ for collection angles below 45°. As previously mentioned, the cavity mode and the PEH-PBI:aPP emission above 45° are no longer spectrally overlapped and the enhancement effect disappears. This behavior is assigned to the spectral redistribution of the oscillator strength caused by the variation of the local density of photonic states within the microcavity.[29]

Besides PL peak enhancement and spectral redistribution, microcavities are also attractive because the possibility of increase of the radiative emission rate of an emitter, whichis represented by the number of emitted photons per unit time, allows more efficient lighting and optical fiber communications.[39] The radiative emission rate can be quantified using the PL enhancement factor (G_e).[39,40] At the cavity mode for normal detection angle ($\theta = 0°$) it can be expressed as Equation (1)[39,40]

$$G_e = \frac{\xi}{2}\frac{\left(1+\sqrt{R_{bottom}}\right)^2\left(1-R_{top}\right)}{\left(1-\sqrt{R_{bottom}R_{top}}\right)^2}\frac{\tau_{cav}}{\tau_{ref}} \quad (1)$$

Table 1. PL QY and PL decay lifetime for the microcavity and for two different references.

Sample		PL QY [%]	Lifetime [ns]
Microcavity	x 20, x 20	≈1	0.6
Reference 1	x 1, x 1	≈1	0.6
Reference 2		≈0.5	0.6

G_e depends on the absolute reflectivity of the mirrors encapsulating the emitting defect layer (R_{top}, R_{bottom}), the radiative lifetime of the emitter in the microcavity and of the reference film (τ_{cav} and τ_{ref}) and the antinode factor (ξ) equals 1 for an emitter homogeneously distributed within the cavity layer.[41] Because R_{top} and R_{bottom} can be hardly evaluated experimentally, they have been retrieved via transfer matrix method calculation (Figure S7, Supporting Information) and resulted $R_{top} \approx 0.92$, and $R_{bottom} \approx 0.88$ at the cavity mode wavelength. To better describe the system, τ_{cav} and τ_{ref} have been assessed comparing the decay lifetime of the microcavity with two reference samples (Figure 5). Reference 1 mimics the dielectric environment of the microcavity and sandwiches the emitting layer with two PAA:PVK bilayers. Reference 2 consists of a PEH-PBI:aPP nanocomposite film cast on a glass substrate. Figure 5a,b shows that the PL decay is monoexponential for all the samples, with a lifetime of 0.6 ns (**Table 1**). Notably, the lifetime does not depend on the measurement wavelength. Indeed, Figure 5a,b shows that the decay is unchanged whether measured at the cavity mode (725 nm, Figure 5a) or at the PEH-PBI:aPP maximum emission (659 nm, Figure 5b). From the ratio between the lifetime of the PEH-PBI:aPP composite and the PEH-PBI monomer (6 ns), we can qualitatively deduce that only few molecules are coherently coupled into a J-aggregate in the PEH-PBI:aPP composite.[5]

Since the microcavity does not induce a substantial variation of the J-aggregates photoluminescence lifetime, $\frac{\tau_{cav}}{\tau_{ref}} = 1$, then $G_e \approx 15$, in agreement with the PL ratio spectra calculated in Figure S6 (Supporting Information) (≈5 at normal incidence). Experimentally, the enhancement disappears for collection angles above 40° because the cavity mode does not overlap the relatively sharp PL spectrum of J-aggregates anymore. In this sense, the relative width of the PBG and of the PL spectrum is an important parameter. Indeed, Figure 4a,b shows that the PBG has a FWHM of ≈60 nm that cannot convey in the cavity mode the full PL spectrum, spanning from 620 to 800 nm. The enhancement is then effective only for about one-third of the overall PEH-PBI:aPP emission spectrum, thus preventing huge effects. As a consequence, integration of G_e over the entire PEH-PBI:aPP spectrum and collection angles (G_{int}, see details in Figure S8, Supporting Information) provides a value below 1 ($G_{int} \approx 0.4$). Therefore, integrated enhancement factors significant for technological applications can be achieved only by improving the PBG-PL relative width, by increasing the dielectric contrast of the polymers used for the DBR mirrors,[42] or by reducing the J-aggregates linewidth that is in compliance

with the number of molecules coherently coupled in the optical transition.[43]

A final remark concerning all-polymer planar microcavities embedding PEH-PBI J-aggregates is related to the possibility to introduce PL quenching defects in the emitter. This phenomenon is well-known to increase the nonradiative recombination rate in inorganic systems, thus reducing the net PL lifetime,[44] and it is often mistaken for Purcell effect. To exclude these effects, we measured the PL QY of PEH-PBI:aPP microcavity and reference sample as reported in Table 1.

The PL QY is ≈1%, for both the microcavity and the Reference 1. Conversely, for Reference 2, made of a bare PEH-PBI:aPP J-aggregates nanocomposite film on glass, the QY is lower and approaches 0.5%. Because all the samples show a monoexponential decay of 0.6 ns, the change in QY cannot be related to a modification of the nonradiative decay rates but only to light extraction efficiency, as often observed.[41,45] Indeed, being the PEH-PBI J-aggregate nanocomposite cladded between two PAA-PVK bilayers, Reference 1 is much more similar to the microcavity than Reference 2.

This result suggests that the fabrication of all-polymer microcavities embedding a complex supramolecular fiber structure like the PEH-PBI J-aggregates one (Figure 1) is reliable and does not introduce defects that could increase nonradiative de-excitation pathways. On the other hand, to achieve integrated rate enhancement requires that three major issues related to the materials have to be overcome: the intrinsic low QY of the emitter, its relatively broad emission spectrum, and the low dielectric contrast between the polymers composing the microcavity DBRs. Indeed, PEH-PBI shows a very high QY in solution, approaching 91% for the monomer (in chloroform) and 86% for the J-aggregate (in cyclohexane). However, when embedded into a nanocomposite at the solid state, this value strongly decreases. Because no evidence for nonfluorescent H-aggregate formation is detectable by spectroscopy,[5,46] this effect may be ascribed to interaggregate interactions in the solid state or to a more efficient triplet generation.

The relatively low dielectric contrast between the DBR components makes the PBG width relatively narrow (≈100 nm), at least with respect to their inorganic counterpart,[36] and strongly affects the enhancement effects. Consequently, processable polymers having larger dielectric contrast have to be developed. Recently, high dielectric contrast polymer systems have been tested, but their processability to microcavity containing a number of layers close to 100 is still an open issue.[42,47]

Notwithstanding these limitations, the results reported confirm that planar microcavities made of commercial polymers allow PL intensity enhancement assigned to the redistribution of the oscillator strength, even for materials challenging to be processed in the solid state such as the PEH-PBI J-aggregates.

3. Conclusions

In this study, we demonstrated that PEH-PBI J-aggregates can be efficiently transferred from solutions to an amorphous polypropylene composite, used as photoactive material in all-polymer microcavities. A systematic characterization of the fluorescence enhancement effects induced by polymer microcavities on PEH-PBI J-aggregates has been reported. The all-polymer microcavity provides a strong and directional spectral redistribution of PEH-PBI J-aggregate fluorescence due to the modified density of photonic states within the microcavity. Analyses of the enhancement factors, the photoluminescence decay, and the quantum yields show that the microcavity growth process does not introduce nonradiative PL de-excitation pathway, being the measured QY limited by light extraction issues only. In order to achieve a full radiative rate enhancement, higher PL QY materials and higher dielectric contrast processable polymers have to be developed.

4. Experimental Section

Synthesis of PEH-PBI: Into the solution of 1,6,7,12-tetrakis(4-hydroxyphenoxy)perylene-3,4:9,10-tetracarboxylic acid bisimide (130 mg, 0.16 mmol),[22] 3,4,5-tris(2-ethylhexyloxy)benzoic acid (350 mg, 0.69 mmol), and DPTS (90.0 mg, 0.32 mmol) in freshly distilled DMF (0.75 mL) and CH_2Cl_2 (1.5 mL) were added 4–5 beads molecular sieves (4 Å) and a solution of DCC (170 mg, 0.82 mmol) in CH_2Cl_2 (0.5 mL) in one portion under argon atmosphere. The reaction mixture was stirred at room temperature for 4 d under argon atmosphere. The solution was concentrated in vacuum and the solid residue was purified by column chromatography on silica with a gradient from CH_2Cl_2 to CH_2Cl_2/Et_2O (1%) followed by the precipitation in cold MeOH and drying under vacuum (50 °C, 10^{-2}–10^{-3} mbar) to give 126 mg (29%) of a dark blue solid.

^1H NMR (400 MHz, $CDCl_3$, ppm): δ = 8.40 (s, 2H), 8.23 (s, 4H), 7.40 (s, 8H), 7.22 (d, 8H, J = 8.44 Hz), 7.02 (d, 8H, J = 10.1 Hz), 3.98–3.90 (m, 24H), 1.79–1.27 (m, 108H), 0.98–0.87 (m, 72H). ^{13}C NMR (100 MHz, $CDCl_3$) δ = 165.1, 162.7, 156.0, 153.3, 152.8, 147.9, 143.2, 133.2, 123.7, 123.6, 123.0, 121.0, 120.8, 120.1, 108.1, 76.2, 71.5, 40.8, 39.7, 30.7, 30.6, 29.4, 29.2, 24.0, 23.8, 23.2, 14.2, 11.3. HRMS (ESI, acetonitrile/chloroform 1:1, pos. mode): m/z calculated for $C_{172}H_{235}N_2O_{28}$ 2776.70209 $[M+H]^+$, found 2776.70213. Elemental analysis (%) calculated for $C_{172}H_{234}N_2O_{28}$ (2777.75): C 74.37, H 8.49, N 1.01; found: C 74.50, H 8.64, N 1.09.

AFM measurement was performed under ambient conditions using a Bruker Multimode 8 SPM system operating in tapping mode in air. Silica cantilevers (OMCL-AC200TS, Olympus) with a resonance frequency of ≈150 kHz and a spring constant of ≈10 N m^{-1} were used. The sample was prepared by spin-coating an *n*-hexane solution (20×10^{-6} M) of PEH-PBI onto silicon wafer (Si-wafer) with 2000 rpm.

FTIR spectra in *n*-hexane solution were recorded with a Jasco FT/IR-4600 spectrometer, using cells with CaF window and path length of 1 mm. Solid-state FTIR spectra were recorded with an AIM-8800 infrared microscope connected to a Shimadzu IR Affinity FT-IR spectrometer. The PEH-PBI sample was prepared as a thin film on a KBr plate (thickness of 2 mm).

The microcavities were fabricated by spin-coating of alternated layers of low and high-index polymer solution. Spin-casting has been already successfully used to prepare multilayered structures of controlled thickness and interfacial roughness of about 1 nm.[34]

Both the DBR mirrors composing the microcavity were grown using poly(acrylic acid) (Sigma Aldrich, MW = 1800) solution in 2-methyl-2-pentanol with concentration of 40 g L^{-1} as low-index medium. The high-index polymer was poly(*N*-vinylcarbazole) (Across Organic, MW = 136 600) dissolved in toluene with concentration of 30 g L^{-1}. Both solutions were spun-cast at 140 RPS. The cavity layer was spun-cast on the first mirror at 70 RPS. The solution was fabricated dissolving ≈5 mg L^{-1} of PEH-PBI in a cyclohexane solution of amorphous polypropylene with concentration of 10 g L^{-1}. Before deposition, *n*-hexane was added dropwise to the polypropylene solution in order to induce PEH-PBI self-assembly.

The reference samples were fabricated using the PEH-PBI:aPP solution used for the microcavity. Reference 2, used for ellipsometric

and photoluminescence measurements, was fabricated by spin-coating deposition on a glass substrate at rotation speed of 70 RPS. Reference 1 was spun-cast at 70 RPS on a PVK-PAA bilayer and then encapsulated with another bilayer consisting of PAA and PVK.

Reflectance, transmittance, and steady-state photoluminescence were measured with optical-fiber setups coupled with a CCD spectrometer (Avantes AvaSpec-2048, 200–1150 nm, resolution 1.4 nm). The white light source was a deuterium–halogen Micropak DH2000BAL, while photoluminescence pumping was provided by a CW laser Oxxius 405 nm, 50 mW.

Time-resolved photoluminescence measurements were recorded using a customized angle-resolved setup coupled to a PicoQuant Time Correlated Single Photon Counting system (Time Harp 260 PICO board, 25 ps temporal resolution; PMA Hybrid 40 detector, 250 ps response time; 405 nm LDH-P-C-405 laser driven with a PDL 800B driver with 5–80 MHz repetition rate) equipped with a compact monochromator (Solar Laser Systems). Photoluminescence lifetimes were retrieved using the PicoQuant FluoFit Pro software, and fitting the PL decay data accounting for instrument response function.

External quantum efficiency measures were performed as described in literature[42,48] using an integrating sphere fiber coupled with a laser excitation source Oxxius[42] 405 nm laser with 90 mW power and a Avantes AvaSpec-2048 spectrometer (200–1150 nm, resolution 1.4 nm). Quantum yield of the PEH-PBI in solutions was measured according to the experimental procedure by using PTI QM-4/2003 spectrofluorometer with additional NIR add-on kit. Fluorescence QYs in solution were determined by optical dilution method (OD_{max} < 0.05) as the average value of four different excitation wavelengths using 5.0 nm slits for both monochromators. *N,N′*-(2,6-di-*iso*-propylphenyl)-1,6,7,12-tetraphenoxyperylene-3,4;9,10-tetracarboxylic acid bisimide (QY = 0.96 ± 0.03 in chloroform)[49] and Rhodamine 800 (QY = 0.25 ± 0.03 in ethanol)[50] were, respectively, used as standards. The signals were corrected for the different refractive index.

Spectroscopic ellipsometry measurements were performed using a VASE instrument by J. A. Woollam Co. in the range (250–2500) nm at different incidence angles from 60° to 75°. Transmittance at normal incidence was also measured with a Varian Cary 6000i spectrometer in the spectral range (300–1800) nm. As a result, the complex dielectric function for all materials was evaluated by WVASE32 software, adopting oscillator models that guarantee for Kramers–Kronig consistency.

Supporting Information

Supporting Information is available from the Wiley Online Library or from the author.

Acknowledgements

Work in Genova and Würzburg was supported by the European Union's Horizon 2020 research and innovation program under the Marie Sklodowska-Curie Grant Agreement No. 643238. Support by the Italian Ministry of University, Research and Instruction through the "Progetti di Ricerca di Rilevante Interesse Nazionale 2010–2011" Program (Materiali Polimerici Nanostrutturati con strutture molecolari e cristalline mirate, per tecnologie avanzate e per l'ambiente, 2010XLLNM3) is also acknowledged. D.C., F.W., P.L., and V.G. conceived the overall project and designed the experiments. P.L. and V.G. worked on the microcavity fabrications. P.L. worked on the microcavity characterization. S.H. developed the PEH-PBI synthesis. S.H. and V.G. elaborated the self-assembly conditions. M.P. performed the ellipsometric measurements and their analysis. Data were analyzed and modeled by P.L., G.M., and D.C. D.C. coordinated the microcavity fabrication and optical characterization activities. G.M. engineered and built the optical setups. The paper was written through contributions of all authors.

Conflict of Interest

The authors declare no conflict of interest.

Keywords

J-aggregates, perylene bisimide, planar microcavities, polymer photonic crystals

Received: June 2, 2017
Revised: July 12, 2017
Published online: August 25, 2017

[1] a) G. Scheibe, L. Kandler, H. Ecker, *Naturwissenschaften* **1937**, *25*, 75; b) E. E. Jelley, *Nature* **1936**, *138*, 1009.
[2] a) F. Würthner, T. E. Kaiser, C. R. Saha-Möller, *Angew. Chem., Int. Ed.* **2011**, *50*, 3376; b) J. Moll, S. Daehne, *J. Chem. Phys.* **1995**, *102*, 6362; c) T. Tani, M. Saeki, Y. Yamaguchi, T. Hayashi, M. Oda, *J. Lumin.* **2004**, *107*, 339; d) V. I. Avdeeva, B. I. Shapiro, *Chem. Mater.* **2003**, *389*, 77; e) H. V. Berlepsch, C. Bottcher, A. Ouart, C. Burger, S. Dahne, S. Kirstein, *J. Phys. Chem. B* **2000**, *104*, 5255; f) J. George, S. Wang, T. Chervy, A. Canaguier-Durand, G. Schaeffer, J.-M. Lehn, J. A. Hutchison, C. Genet, T. W. Ebbesen, *Faraday Discuss.* **2015**, *178*, 281; g) E. Collini, C. Ferrante, R. Bozio, *J. Phys. Chem. B* **2005**, *109*, 2.
[3] S. K. Semion, A. Eisfeld, S. Valleau, A. Aspuru-Guzik, *Nanophotonics* **2013**, *2*, 21.
[4] F. C. Spano, S. Mukamel, *J. Chem. Phys.* **1989**, *91*, 683.
[5] a) T. Kobayashi, *J-Aggregates*, World Scientific, Singapore **2012**; b) T. Kobayashi, *J-Aggregates*, World Scientific, Singapore **1996**.
[6] C. Xue, Y. Xue, L. Dai, A. Urbas, Q. Li, *Adv. Opt. Mater.* **2013**, *1*, 581.
[7] a) C. Xue, O. Birel, Y. Xue, L. Dai, A. Urbas, Q. Li, *J. Phys. Chem. C* **2013**, *117*, 6752; b) C. Xue, O. Birel, M. Gao, S. Zhang, L. Dai, A. Urbas, Q. Li, *J. Phys. Chem. C* **2012**, *116*, 10396.
[8] a) J. R. Tischler, M. S. Bradley, V. Bulovic, J. H. Song, A. Nurmikko, *Phys. Rev. Lett.* **2005**, *95*, 036401; b) B. Stender, S. F. Völker, C. Lambert, J. Pflaum, *Adv. Mater.* **2013**, *25*, 2943.
[9] a) S. Özçelik, D. L. Akins, *Appl. Phys. Lett.* **1997**, *71*, 3057; b) S. Özçelik, I. Özçelik, D. L. Akins, *Appl. Phys. Lett.* **1998**, *73*, 1949.
[10] a) C. Chen, R. Wang, L. Guo, N. Fu, H. Dong, Y. Yuan, *Org. Lett.* **2011**, *13*, 1162; b) J. Sloniec-Myszk, U. Resch-Genger, A. Hennig, *J. Phys. Chem. B* **2016**, *120*, 877.
[11] a) N. Eradat, A. Y. Sivachenko, M. E. Raikh, Z. V. Vardeny, A. A. Zakhidov, R. H. Baughman, *Appl. Phys. Lett.* **2002**, *80*, 3491; b) V. M. Agranovich, M. Litinskaia, D. G. Lidzey, *Phys. Rev. B* **2003**, *67*, 085311; c) R. B. Fletcher, D. G. Lidzey, D. D. C. Bradley, M. Bernius, S. Walker, *Appl. Phys. Lett.* **2000**, *77*, 1262; d) S. Pirotta, M. Patrini, M. Liscidini, M. Galli, G. Dacarro, G. Canazza, G. Guizzetti, D. Comoretto, D. Bajoni, *Appl. Phys. Lett.* **2014**, *104*, 4051111.
[12] a) F. Marabelli, D. Comoretto, D. Bajoni, M. Galli, L. Fornasari, *Mater. Res. Soc. Symp. Proc.* **2005**, *846*, DD12.11.1; b) C. Huang, S. Barlow, S. R. Marder, *J. Org. Chem.* **2011**, *76*, 2386; c) X. Zhan, A. Facchetti, S. Barlow, T. J. Marks, M. A. Ratner, M. R. Wasielewski, S. R. Marder, *Adv. Mater.* **2011**, *23*, 268.
[13] a) F. Würthner, C. R. Saha-Möller, B. Fimmel, S. Ogi, P. Leowanawat, D. Schmidt, *Chem. Rev.* **2016**, *116*, 962; b) H. Langhals, J. Karolin, L. B.-A. Johansson, *J. Chem. Soc., Faraday Trans.* **1998**, *94*, 2919.
[14] a) M. Sadrai, L. Hadel, R. R. Sauers, S. Husain, K. Krogh-Jespersen, J. D. Westbrook, G. R. Bird, *J. Phys. Chem.* **1992**, *96*, 7988; b) H. G. Löhmannsröben, H. Langhals, *Appl. Phys. B* **1989**, *48*, 449; c) M. Sadrai, G. R. Bird, *Opt. Commun.* **1984**, *51*, 62.

[15] P. Osswald, F. Würthner, *J. Am. Chem. Soc.* **2007**, *129*, 14319.
[16] a) M. G. Ramírez, S. Pla, P. G. Boj, J. M. Villalvilla, J. A. Quintana, M. A. Díaz-García, F. Fernández-Lázaro, Á. Sastre-Santos, *Adv. Opt. Mater.* **2013**, *1*, 933; b) L. Cerdan, A. Costela, G. Duran-Sampedro, I. Garcia-Moreno, M. Calle, M. Juan-y-Seva, J. de Abajo, G. A. Turnbull, *J. Mater. Chem.* **2012**, *22*, 8938; c) M. A. Díaz-García, E. M. Calzado, J. M. Villalvilla, P. G. Boj, J. A. Quintana, F. J. Céspedes-Guirao, F. Fernández-Lázaro, Á. Sastre-Santos, *Synth. Met.* **2009**, *159*, 2293.
[17] M.-J. Lin, Á. J. Jiménez, C. Burschka, F. Würthner, *Chem. Commun.* **2012**, *48*, 12050.
[18] a) M. Kasha, H. R. Rawls, M. Ashraf El-Bayoumi, *Pure Appl. Chem.* **1965**, *11*, 371; b) N. J. Hestand, F. C. Spano, *J. Chem. Phys.* **2015**, *143*, 244707.
[19] Z. Chen, B. Fimmel, F. Würthner, *Org. Biomol. Chem.* **2012**, *10*, 5845.
[20] J. Sung, P. Kim, B. Fimmel, F. Würthner, D. Kim, *Nat. Commun.* **2015**, *6*, 8646.
[21] T. E. Kaiser, V. Stepanenko, F. Würthner, *J. Am. Chem. Soc.* **2009**, *131*, 6719.
[22] a) M. G. Ramírez, M. Morales-Vidal, V. Navarro-Fuster, P. G. Boj, J. a. Quintana, J. M. Villalvilla, A. Retolaza, S. Merino, M. A. Díaz-García, *J. Mater. Chem. C* **2013**, *1*, 1182; b) E. M. Calzado, J. M. Villalvilla, P. G. Boj, J. A. Quintana, R. Gómez, J. L. Segura, M. A. Díaz-García, *J. Phys. Chem. C* **2007**, *111*, 13595; c) E. M. Calzado, J. M. Villalvilla, P. G. Boj, J. A. Quintana, R. Gómez, J. L. Segura, M. A. Díaz García, *Appl. Opt.* **2007**, *46*, 3836.
[23] a) S. Herbst, B. Soberats, P. Leowanawat, M. Lehmann, F. Würthner, *Angew. Chem., Int. Ed.* **2017**, *56*, 2162; b) Z. Yu, Y. Wu, Q. Liao, H. Zhang, S. Bai, H. Li, Z. Xu, C. Sun, X. Wang, J. Yao, H. Fu, *J. Am. Chem. Soc.* **2015**, *137*, 15105; c) L. Tropf, C. P. Dietrich, S. Herbst, A. L. Kanibolotsky, P. J. Skabara, F. Würthner, I. D. W. Samuel, M. C. Gather, S. Höfling, *Appl. Phys. Lett.* **2017**, *110*, 153302.
[24] a) M. G. Ramírez, M. Morales-Vidal, V. Navarro-Fuster, P. G. Boj, J. a. Quintana, J. M. Villalvilla, A. Retolaza, S. Merino, M. A. Díaz-García, *J. Mater. Chem. C* **2013**, *1*, 1182; b) E. M. Calzado, J. M. Villalvilla, P. G. Boj, J. A. Quintana, R. Gómez, J. L. Segura, M. A. Díaz-García, *J. Phys. Chem. C* **2007**, *111*, 13595; c) E. M. Calzado, J. M. Villalvilla, P. G. Boj, J. A. Quintana, R. Gómez, J. L. Segura, M. A. Díaz García, *Appl. Opt.* **2007**, *46*, 3836.
[25] M. Signoretto, N. Zink-Lorre, I. Suárez, E. Font-Sanchis, Á. Sastre-Santos, V. S. Chirvony, F. Fernández-Lázaro, J. P. Martínez-Pastor, *ACS Photonics* **2017**, *4*, 114.
[26] a) S. Chénais, S. Forget, *Polym. Int.* **2012**, *61*, 390; b) W. Zhang, J. Yao, Y. S. Zhao, *Acc. Chem. Res.* **2016**, *49*, 1691; c) A. J. C. Kuehne, M. C. Gather, *Chem. Rev.* **2016**, *116*, 12823.
[27] a) L. Berti, M. Cucini, F. Di Stasio, D. Comoretto, M. Galli, F. Marabelli, N. Manfredi, C. Marinzi, A. Abbotto, *J. Phys. Chem. C* **2010**, *114*, 2403; b) L. Fornasari, F. Floris, M. Patrini, G. Canazza, G. Guizzetti, D. Comoretto, F. Marabelli, *Appl. Phys. Lett.* **2014**, *105*, 053303.
[28] L. Frezza, M. Patrini, M. Liscidini, D. Comoretto, *J. Phys. Chem. C* **2011**, *115*, 19939.
[29] G. Canazza, F. Scotognella, G. Lanzani, S. De Silvestri, M. Zavelani-Rossi, D. Comoretto, *Laser Phys. Lett.* **2014**, *11*, 035804.
[30] R. J. Knarr III, G. Manfredi, E. Martinelli, M. Pannocchia, D. Repetto, C. Mennucci, I. Solano, M. Canepa, F. Buatier de Mongeot, G. Galli, D. Comoretto, *Polymer* **2016**, *84*, 383.
[31] a) P. Lova, C. Bastianini, P. Giusto, M. Patrini, P. Rizzo, G. Guerra, M. Iodice, C. Soci, D. Comoretto, *ACS Appl. Mater. Interfaces* **2016**, *8*, 31941; b) P. Lova, G. Manfredi, L. Boarino, A. Comite, M. Laus, M. Patrini, F. Marabelli, C. Soci, D. Comoretto, *ACS Photonics* **2015**, *2*, 537; c) P. Lova, G. Manfredi, L. Boarino, M. Laus, G. Urbinati, T. Losco, F. Marabelli, V. Caratto, M. Ferretti, M. Castellano, C. Soci, D. Comoretto, *Phys. Status Solidi C* **2014**, *12*, 158; d) G. Manfredi, C. Mayrhofer, G. Kothleitner, R. Schennach, D. Comoretto, *Cellulose* **2016**, *23*, 2853.
[32] a) H. Song, K. Singer, J. Lott, Y. Wu, J. Zhou, J. Andrews, E. Baer, A. Hiltner, C. Weder, *J. Mater. Chem.* **2009**, *19*, 7520; b) K. D. Singer, T. Kazmierczak, J. Lott, H. Song, Y. Wu, J. Andrews, E. Baer, A. Hiltner, C. Weder, *Opt. Express* **2008**, *16*, 10358; c) T. Kazmierczak, H. Song, A. Hiltner, E. Baer, *Macromol. Rapid Commun.* **2007**, *28*, 2210; d) D. Comoretto, *Organic and Hybrid Photonic Crystals*, Springer, Cham, Switzerland **2015**.
[33] H. Lin, R. Camacho, Y. Tian, T. E. Kaiser, F. Würthner, I. G. Scheblykin, *Nano Lett.* **2010**, *10*, 620.
[34] K. Unger, R. Resel, C. Czibula, C. Ganser, C. Teichert, G. Jakopic, G. Canazza, S. Gazzo, D. Comoretto, presented at *6th Int. Conf. Transparent Optical Networks (ICTON 2014)*, Graz, Austria, **2014**.
[35] L. Fornasari, F. Floris, M. Patrini, D. Comoretto, F. Marabelli, *Phys. Chem. Chem. Phys.* **2016**, *18*, 14086.
[36] S. Gazzo, G. Manfredi, R. Poetzsch, Q. Wei, M. Alloisio, B. Voit, D. Comoretto, *J. Polym. Sci., Part B: Polym. Phys.* **2016**, *54*, 73.
[37] F. Scotognella, S. Varo, L. Criante, S. Gazzo, G. Manfredi, R. J. Knarr III, D. Comoretto, *Organic and Hybrid Photonic Crystals*, Springer, Cham, Switzerland **2015**.
[38] S. E. Burns, G. Denton, N. Tessler, M. A. Stevens, F. Cacialli, R. H. Friend, *Opt. Mater.* **1998**, *9*, 18.
[39] E. F. Schubert, N. E. J. Hunt, M. Micovic, R. J. Malik, D. L. Sivco, A. Y. Cho, G. J. Zydzik, *Science* **1994**, *265*, 943.
[40] a) N. E. J. Hunt, E. F. Schubert, R. F. Kopf, D. L. Sivco, A. Y. Cho, G. J. Zydzik, *Appl. Phys. Lett.* **1993**, *63*, 2600; b) J. Grüner, F. Cacialli, R. H. Friend, *J. Appl. Phys.* **1996**, *80*, 207.
[41] H. Benisty, H. D. Neve, C. Weisbuch, *IEEE J. Quantum Electron.* **1998**, *34*, 1612.
[42] G. Manfredi, P. Lova, F. Di Stasio, R. Krahne, D. Comoretto, *ACS Photonics* **2017**, *4*, 1761.
[43] E. W. Knapp, *Chem. Phys.* **1984**, *85*, 73.
[44] T. Baba, D. Sano, *IEEE J. Sel. Top. Quantum Electron.* **2003**, *9*, 1340.
[45] a) D. Z. Garbuzov, S. R. Forrest, A. G. Tsekoun, P. E. Burrows, V. Bulović, M. E. Thompson, *J. Appl. Phys.* **1996**, *80*, 4644; b) G. Gu, D. Z. Garbuzov, P. E. Burrows, S. Venkatesh, S. R. Forrest, M. E. Thompson, *Opt. Lett.* **1997**, *22*, 396.
[46] M. v. Burgel, D. A. Wiersma, K. Duppen, *J. Chem. Phys.* **1995**, *102*, 20.
[47] S. Padhmanabhan, S. V. Radice, D. Comoretto, S. Gazzo, Int. Patent WO2016/087439 A1, **2016**.
[48] a) J. C. de Mello, H. F. Wittmann, R. H. Friend, *Adv. Mater.* **1997**, *9*, 230; b) N. C. Greenham, I. D. W. Samuel, G. R. Hayes, R. T. Phillips, Y. A. R. R. Kessener, S. C. Moratti, A. B. Holmes, R. H. Friend, *Chem. Phys. Lett.* **1995**, *241*, 89.
[49] R. Gvishi, R. Reisfeld, Z. Burshtein, *Chem. Phys. Lett.* **1993**, *213*, 338.
[50] A. Alessi, M. Salvalaggio, G. Ruzzon, *J. Lumin.* **2013**, *134*, 385.